Dynamic Heterogeneities in Liquid Mixtures Confined in Nanopores

Ramona Mhanna,[†,§] Pierre Catrou,[†] Sujeet Dutta,[†] Ronan Lefort,[†] Ilham Essafri,[†] Aziz Ghoufi,[†] Matthias Muthmann,[‡] Michaela Zamponi,[‡] Bernhard Frick,[§] Denis Morineau[†*]

[†]Institute of Physics of Rennes, CNRS-University of Rennes 1, UMR 6251, F-35042 Rennes, France

[§] Institut Laue-Langevin, 71 avenue des Martyrs, F-38000 Grenoble, France

[‡] Forschungszentrum Jülich GmbH, Jülich Centre for Neutron Science at MLZ

Lichtenbergstr. 1, 85748 Garching, Germany

Corresponding Author

* E-mail: denis.morineau@univ-rennes1.fr

ABSTRACT: Binary liquid mixtures can exhibit nanosegregation, albeit being fully miscible and homogeneous at the macroscopic scale. This tendency can be amplified by geometrical nanoconfinement, leading to remarkable properties. This work investigates the molecular dynamics of *tert*-Butanol (TBA)-Toluene (TOL) mixtures confined in silica nanochannels by quasielastic neutron scattering and molecular dynamics simulation. It reveals a decoupling of the molecular motion of each constituent of the binary liquid, which can be followed independently by selective isotopic HD labelling. We argue that this behavior is the signature of spatially

segregated dynamic heterogeneities, which are due to the recently established core-shell nanophase separation induced by mesoporous confinement.

INTRODUCTION

The dynamics of nanoconfined liquids has been a topic of extensive research activities since the pioneering studies of the early 90s.[1-5] A wealth of fundamental knowledge about pure nanoconfined liquids has been collected and are subject of review articles.[6-15] However, it turns out that liquid mixtures, which are particularly relevant for applications, may exhibit uncommon behaviors with respect to most studied pure systems. Fundamentally, a few studies on models systems, comprising fully miscible binary liquids confined in mesostructured porous matrices have addressed this question. The dynamics of aqueous alcohol solutions confined in MCM-41 were studied by MD simulations, dielectric spectroscopy and calorimetry experiments.[16-18] These studies provide evidence of the possible microphase separation of fully miscible mixtures in a confined environment. More specifically, the seemingly abnormal dependence of the liquid dynamics on the concentration has been attributed to the segregation of a part of the water molecules at the pore surface, leading to an actually higher local concentration of solutes in the confined solution. As a result, two important issues emerge that are yet to be addressed experimentally: First, can direct confirmation and structural characterization of confinement-induced microphase separation be provided? Second, can one disentangle distinct dynamics that would be related to segregated molecules in the two distinct regions in the pore?

To answer the first question, we have recently reported the microphase separation of fully miscible blends of *tert*-Butanol (TBA) - Toluene (TOL) liquids confined in the cylindrical nanochannels of MCM-41 and SBA-15 mesoporous silicates (diameter D = 3.65 nm and 8.3 nm respectively).[19-22] We carried out extensive structural analysis using carefully designed neutron diffraction experiments with hydrogen/deuterium isotopic substitution.[21, 22] The measured inhomogeneous radial concentration profile demonstrates that the structure comprises a cylindrical

organization of two concentric core-shell regions of different compositions in which TBA molecules segregate on the surface of the pores, forming an interfacial region surrounding a TOL-rich core. The condition of formation of such structures was recently linked to different interfacial interactions quantified experimentally by modelling the thermodynamics of binary gas adsorption.[23] This observation was also confirmed by a molecular dynamics simulation study, which brought a deeper insight on this phenomenon at the molecular scale.[24]

This direct experimental evidence of the core-shell organization represents a unique insight to allow the investigation of the particular dynamical properties of these novel systems. Indeed, we evaluated the phase behavior and the glassy dynamics of TBA-TOL binary liquids confined in MCM-41 by the combination of neutron diffraction and differential scanning calorimetry (DSC) measurements in an attempt to examine the thermal behavior of this unusual phase in terms of density and heat capacity.[25] Our studies revealed the co-existence of two different glass transitions, which suggests the existence of two spatially separated dynamics, likely attributed to the subcomponents of the microphase separated mixture. Although significant, this pursue to link the unusual structural and dynamic properties of confined binary liquids is limited by the non-specific character of calorimetry, implying that a distinction between the dynamics of the two constituents has not yet been realized.

In the present study, we independently measured the dynamics of TBA and TOL molecules and interpret the observed variation in light of the core-shell structure they adopt in the nanochannels. In addition, we extend the investigated timescale of the dynamics from seconds (glassy dynamics around T_g) to the nanoseconds (microscopic molecular motion). To achieve this objective we conducted high-resolution quasi-elastic neutron scattering experiments on liquids confined in SBA-15 with different isotopic compositions. Using this technique and contrast variation, the

dynamics of the hydrogenated component was highlighted due to its high incoherent cross section, while the contribution from the complementary molecule was minimized by deuteration. The experimental findings are discussed in the light of recent MD simulation results.

METHODS

Samples. The hydrogenated solvents TBA and TOL (>99%) were purchased from Sigma-Aldrich and the fully deuterated solvents TBA ($C_4D_{10}O$, 99.8%) and TOL (C_7D_8, 99.5%) were obtained from Eurisotop and used directly, without further purification. The SBA-15 mesoporous silicates were prepared in our laboratory using a procedure similar to that described elsewhere,[8, 15, 26-28] with slight modifications of the thermal treatments to optimize the final structure of the product.[29] Nonionic triblock copolymer (Pluronic P_{123}): $(EO)_{20}(PO)_{70}(EO)_{20}$ was used as a template to obtain a mesostructured triangular array of aligned channels with a pore diameter D = 8.3 nm, confirmed by nitrogen adsorption, transmission electron microscopy and neutron diffraction. The calcinated matrix was dried at 120°C under primary vacuum for 12 hours before experiments.

DSC Experiments. For DSC measurements, SBA-15 samples were filled by liquid imbibition with the appropriate weighted amount of fully hydrogenated TBA-TOL mixtures to allow the full loading of the porous volume V_P = 1 cm^3 g^{-1}, as measured by nitrogen adsorption, and hermetically sealed in aluminum pans. The measurements were performed on a TA Instrument Q20 DSC. The thermograms were recorded at a heating rate of 10 K min^{-1} after cooling the sample from 320 K to 100 K.

Quasielastic Neutron Scattering. QENS experiments were conducted on the backscattering instrument SPHERES operated by JCNS at the Heinz Maier-Leibnitz Zentrum (MLZ) (Garching,

Germany), at a fixed incoming wavelength of 6.27 Å, using Si (111) crystals as monochromator and analyzers.[30, 31] The resulting energy resolution is about 0.65 μeV (FWHM) and the investigated momentum transfer (Q)-range 0.16-1.8 $Å^{-1}$. However the analysis was limited to $Q > 0.4$ $Å^{-1}$ because of contributions at lower Q values due to intense coherent scattering from the Bragg reflections of the mesoporous structure. Elastic Fixed Window Scans (EFWSs) with the monochromator Doppler drive at rest were measured during a slow heating scan at a rate of 0.75 $K.min^{-1}$ from about 5 K to 360 K, accumulating data points for elastic scattering over 2 minutes (i.e. $\Delta T \approx 1.5$ K).

Sample preparation was similar for all the confined samples. A constant amount of the mesoporous materials (SBA-15) was filled into a standard flat aluminum cell for bulk and confined samples. Liquid binary mixtures (prepared in volume fraction for different isotopic and concentration compositions) were filled using a calibrated micropipette. The targeted filling was equal to 100% of the pore volume of the confinement matrix which was determined by adsorption isotherm measurements ($V_P = 1$ cm^3 g^{-1}). An indium wire was used to seal the sample cell. Finally, the samples were allowed to equilibrate for a few hours to ensure the homogeneous filling of the different pores, in accordance with the SANS kinetic measurements.[22] In order to reduce multiple scattering, the thickness of the sample was chosen to be 1mm resulting in a transmission of typically 90% depending on the density and exact composition of the sample. Spectra were grouped, corrected for detector efficiency, empty cell and empty matrices contributions according to standard procedures using the *Slaw* software and internal routines. The corrected spectra were then normalized to the intensity measured at the lowest temperature, considering that the incoherent scattering is entirely contained in the elastic resolution under such conditions.

No sign of crystallization was observed in the DSC and QENS experiments, consistent with the absence of bulk excess liquid outside the matrix. The pores are thus completely filled, in agreement with previous studies using the same filling method.[22, 25]

Molecular Dynamics Simulations. The simulation method is the same as used in ref. 24. A silica cylindrical nanopore of diameter D = 24 Å with a hydrophilic surface included in a cubic silica cell of 35.7 Å was obtained by applying the process proposed by Bródka and Zerda.[32] We generated a cylindrical cavity along the z axis of the cubic silica cell of 35.7 Å by removing the atoms within a cylinder of diameter (D) 24 Å. From their coordination numbers, we distinguished bridging oxygen (Ob) bonded to two silicon atoms from non-bridging oxygens (Onb) bonded to only one silicon and bonded to one hydrogen atom (Hnb). An iterative procedure of atom (O and Si) removal was applied until only tetra-coordinated silicon atoms, bonded to a maximum of two Onbs, were present in the structure. Finally, non-bridging oxygens were saturated with hydrogen atoms to form surface hydroxyl groups. The inner surface coverage of silanol groups was about 7.5 nm^{-2}. The silica matrix was subsequently kept rigid, except for the rotation around the Si-O bond of the hydroxyl groups, which was allowed using the SHAKE constraints algorithm with the distance between the oxygen and hydrogen atoms fixed at 1.09 Å.

Intermolecular interactions are the sum of both electrostatic and dispersive–repulsive Lennard-Jones contributions. The silica framework was modeled using the ClayFF force field.[33] The TBA and TOL systems were modeled using the flexible non-polarizable OPLS force field with all atoms (AA).[34] Whereas the intramolecular contributions (bonds, bending, and dihedral angles) were conserved as original, the partial charges were calculated using ab-initio calculations. Van der Waals interactions between TOL and TBA were calculated using the Lorentz-Berthelot mixing rules. The LJ parameters between the silica nanopore and the TOL molecules have been optimized

to qualitatively reproduce the experimental isotherms.[24] The so-optimized interactions between TOL molecules and silica material are provided in Table 1. Force field parameters of silica material, TOL, and TBA and crossed interactions are provided in the FIELD.txt file of DL_POLY software.[35]

Table 1. Crossed Lennard-Jones parameters. CH_3 is the carbon of the methyl groups of toluene, CH the carbon of the CH groups of toluene, and C the carbon without hydrogen atoms in toluene

	σ (Å)	**ε (K)**
Si-CH_3	3.6475	46.17061
Si-CH	3.6725	47.54915
Si-C	3.6725	47.54915

The MD simulations were performed using a time step of 0.002 ps to sample 10 ns (acquisition phase) with an initial configuration obtained from GCMC simulation at saturation vapor pressure and at 308 K. The number of confined TBA and TOL molecules were N_{TOL} = 84, 64 and N_{TBA} = 98, 22 for the pure liquids and the binary mixture (x_{TBA} = 0.24), respectively. The equilibration time corresponded to 10 ns. All MD simulations were performed with the DL_POLY package using the velocity-Verlet algorithm combined with the Nose-Hoover thermostat.[36, 37]

RESULTS AND DISCUSSION

Differential Scanning Calorimetry. The phase behavior of the samples was determined by DSC. The thermograms are shown in Figures 1a and 1b for the bulk and confined liquid

respectively. They were obtained by heating at 10 K.min^{-1}, after a pre-cooling scan at the same rate. It is well-known that under mild cooling conditions TOL generally forms a glass. The glass transition is identified during heating by a jump in the heat flow, indicating an increase in heat capacity, at a temperature noted T_g (121.5 K) in Figure 1a. It is followed by a sharp exothermic peak at T_c (144 K) and an endothermic peak at T_m (180 K) during the subsequent heating, which correspond to the cold crystallization and melting transitions, respectively. In contrast, TBA cannot be vitrified, but crystallizes readily under normal cooling conditions. This behavior is confirmed in Figure 1b, by the two endothermic peaks attributed, according to McGregor et al, to the solid−solid transition between the trigonal $P\bar{3}$ phase (phase II) and the triclinic $P\bar{1}$ (phase IV) at T_s = 268 K and the subsequent melting of the triclinic $P\bar{1}$ phase (phase IV) at T_m = 290 K.[38]

The thermograms measured for the confined systems are very different from those of the bulk, as shown in Figure 1a. The first observation is the absence of exo- or endothermic peak, which means that crystallization has been hindered by confinement. The pure confined liquids TOL and TBA exhibit a glass transition at temperatures of T_g^{TOL} = 118 K and T_g^{TBA} = 185 K, respectively. For TBA, the heat capacity jump is spread over a wide temperature range (more than 20 K), indicating a broadening of the distribution of relaxation times in the confined state. This probably reflects the inhomogeneity of the environments experienced by the molecules located from the pore surface to the center of the pore. For TOL, a tiny step around 130 K is perceived and, if real, could be related to the thermal response of the interfacial layer, a phenomenon which has been already observed for ortho-terphenyl confined in SBA-15.[39] For the binary liquid mixture, the most interesting result emerges from the observation of two distinct jumps of heat capacity with comparable amplitudes. These correspond to glass transitions centered around T_g^1 = 120 K and T_g^2 = 158 K. This result is similar to recent observations made for TBA-TOL mixtures confined in

MCM-41 materials (3.6 nm pore size).[25] They were interpreted in terms of two glass transitions arising from the TOL-rich and TBA–rich phases, forming respectively the core and the shell of the microphase separated liquid. It is interesting to note that the two glass transitions are sharper and better resolved in the present case, which is possibly a consequence of the larger pore size of SBA-15 compared to that of MCM-41. This provided good conditions for the aimed disentangling of core and shell contributions of the molecular dynamics of TOL and TBA molecules, as discussed below.

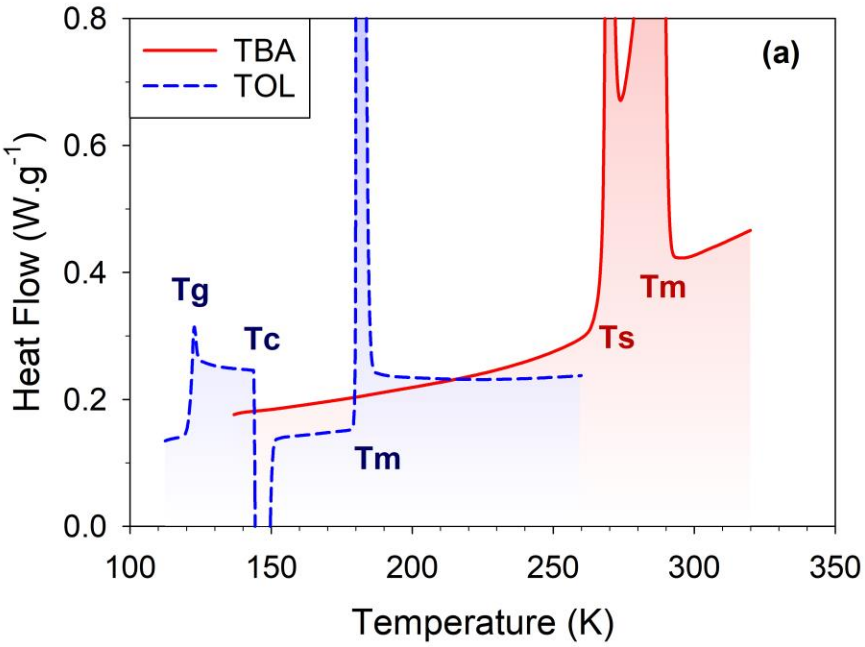

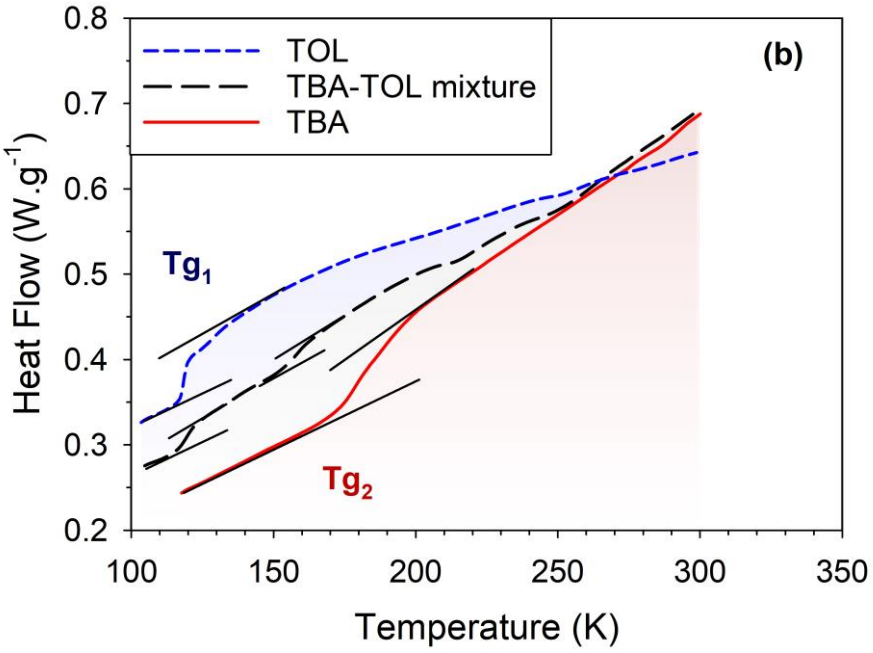

Figure 1. DSC thermograms on heating of toluene (TOL, blue dashed line) and *tert*-Butanol (TBA, red solid line) (a) in the bulk state and (b) in confinement in SBA-15. In (b), the thermogram of the TBA-TOL confined binary mixture is also added (long dashed black line). The jumps in heat capacity are underlined by thin tangential black lines just before and after each glass transition.

Elastic Fixed Window Scans. In the limit of small energy transfer, which corresponds to the quasi-elastic range, the incoherent neutron scattering function (also called dynamic structure factor) is commonly approximated by

$$S_{incoh}(Q,\omega) = e^{\frac{-\langle r^2\rangle Q^2}{6}}\left[A(Q)\delta(\omega) + \left(1 - A(Q)\right) S_{quasi}(Q,\omega)\right] \qquad (1)$$

The first term is known as the Debye-Waller factor and corresponds to the modes of vibration, where $\langle r^2\rangle$ is the mean squared displacement (*i.e.* twice the value of $\langle u^2\rangle$, the mean squared offset of atomic positions from their equilibrium positions), $A(Q)$ is the amplitude of the pure elastic

component (often noted EISF, for the Elastic Incoherent Structure Factor) describing the geometry of localized motions and $S_{quasi}(Q,\omega)$ is the quasi-elastic component.[40]

EFWS measurements are obtained by counting the elastic fraction of the dynamic structure factor that is contained in the energy resolution of the spectrometer according to

$$I^{EFWS}(Q) = \frac{[S(Q,\omega)\otimes R(Q,\omega)](\omega=0)}{[S_{T=0}(Q,\omega)\otimes R(Q,\omega)](\omega=0)} \approx \frac{\langle S(Q,\omega)\rangle_{\Delta\omega}}{\langle S_{T=0}(Q,\omega)\rangle_{\Delta\omega}} \quad (2)$$

where $R(Q,\omega)$ is the resolution function of the instrument and $\Delta\omega$ is the corresponding energy resolution width (FWHM). This quantity can be seen as the value of $S(Q, \omega)$, normalized to a zero temperature and averaged over a narrow energy range $\Delta\omega$ (typically $\Delta\omega = 1\mu eV$) around the elastic peak. This equivalence would be strictly valid if the resolution function was a gate function. As a result, EFWS give the dependence of the dynamics as a function of the temperature at the nanosecond timescale. The EFWSs values measured for the two pure hydrogenated liquids TOL and TBA are illustrated in Figures 2a-b.

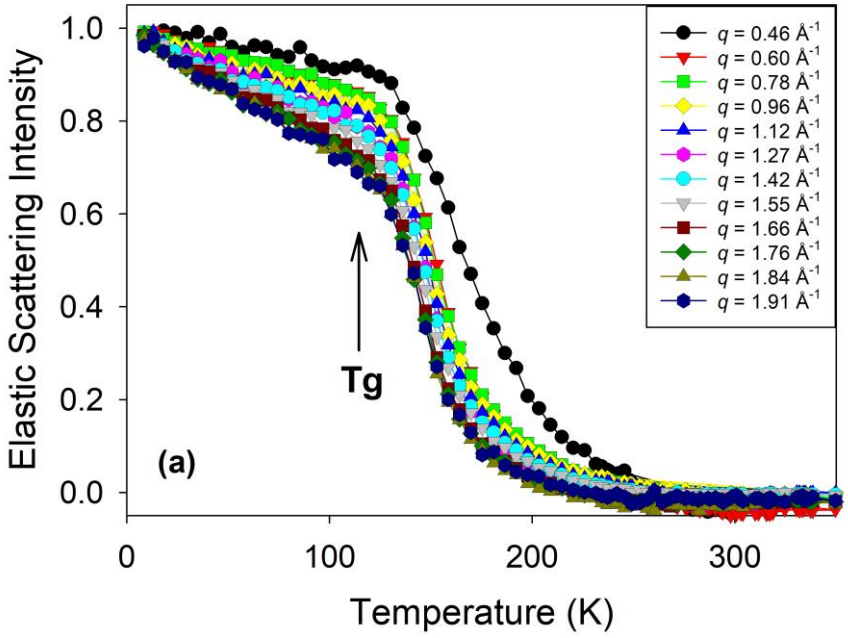
Elastic Scattering Intensity
1.0
0.8
0.6
0.4
0.2
0.0
0
100
200
300
Temperature (K)
Tg
(a)
q = 0.46 Å-1
q = 0.60 Å-1
q = 0.78 Å-1
q = 0.96 Å-1
q = 1.12 Å-1
q = 1.27 Å-1
q = 1.42 Å-1
q = 1.55 Å-1
q = 1.66 Å-1
q = 1.76 Å-1
q = 1.84 Å-1
q = 1.91 Å-1

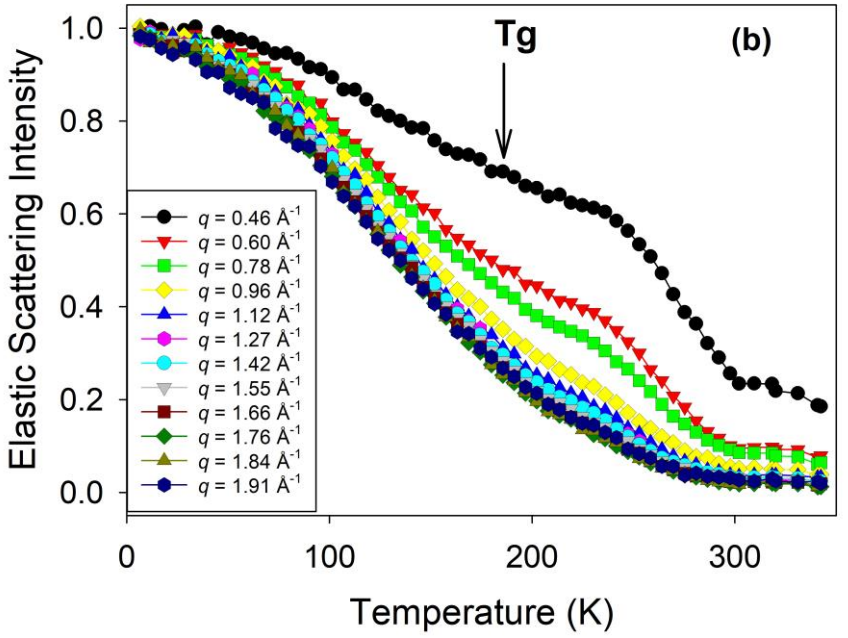
Elastic Scattering Intensity
1.0
0.8
0.6
0.4
0.2
0.0
0
100
200
300
Temperature (K)
Tg
(b)
q = 0.46 Å-1
q = 0.60 Å-1
q = 0.78 Å-1
q = 0.96 Å-1
q = 1.12 Å-1
q = 1.27 Å-1
q = 1.42 Å-1
q = 1.55 Å-1
q = 1.66 Å-1
q = 1.76 Å-1
q = 1.84 Å-1
q = 1.91 Å-1

Figure 2. Elastic fixed window scans of fully hydrogenated (a) TOL and (b) TBA confined in SBA-15. The different curves correspond to different values of the momentum transfer *Q* ranging from 0.46 $Å^{-1}$ (upper curve) to 1.91 $Å^{-1}$ (lower curve).

For TOL, one can notice below T_g a gradual decrease of intensity during heating, which is primarily due to the Debye-Waller factor since the quasi-elastic contribution of most other modes is too slow to be distinguished from a purely elastic line. Upon further heating (above 140 K, a few tens of degrees above T_g), the intensity decreases readily to reach tiny values (< 0.1) at 200 K. This second faster decay is attributed to the onset of quasi-elastic modes (such as molecular rotation or translation), whose broadening exceeds the instrumental resolution. For TBA, there is a more pronounced decrease in the elastic intensity already at temperatures below T_g, despite its higher value compared to TOL. This indicates that the protons of TBA are already involved in fast motions (secondary modes) deep within the vitreous state. These are likely related to methyl rotations as well as tumbling and rotation of the whole molecule, favored by its globular shape.

Table 2. Incoherent Scattering Cross sections of the two studied molecules as a function of their isotopic composition.

Incoherent Scattering Cross Section (10^{-24} cm^2)	**TOL**	**TBA**
Hydrogenated	639	799
Deuterated	16	20

We now consider the confined binary liquids for which isotopic substitution has been applied to label the hydrogenated molecules and magnify their dynamics. Due to the high value of the incoherent scattering cross section of hydrogen atoms, the hydrogenated molecules are expected to scatter much more than their deuterated equivalents, as indicated by the molecular cross sections shown in Table 2. This effect is illustrated in Figure 3 for the case of a TBA/TOL mixture with equimolar composition (i.e. $x_{TBA} = 0.5$). Three different isotopic compositions were considered, combining hydrogenated or deuterated molecules. They are subsequently denoted TBA(H)/TOL(H), TBA(D)/TOL(H), and TBA(H)/TOL(D) mixtures.

From a comparison of Figures 3a-c, it is clear that EFWSs depend on the isotopic composition. Figure 3a corresponds to the fully hydrogenated mixture TBA(H)/TOL(H), where the two molecules contribute almost equally to the scattered intensity. The contribution of TOL is amplified for the TBA(D)/TOL(H) sample, as shown in Figure 3b, which results in a rather marked decrease in the elastic intensity above about 140 K, qualitatively resembling the case of pure TOL. On the contrary, for TBA(H)/TOL(D), the decay of the elastic intensity illustrated in Figure 3c is more gradual and extends to a higher temperature (*i.e.* above 300 K). This dependence of the elastic intensity on the nature of the labelled molecule (TBA or TOL) indicates that the TBA and TOL molecules undergo different dynamics in the liquid mixture. This is also consistent with the observation of two previously discussed glass transition temperatures, which have been attributed to the TBA-rich and TOL-rich regions, respectively. The curves presented in Figure 3d were computed as the weighed sums of the EFWSs of the two pure hydrogenated systems. Their similarity with the experimental EFWSs of the fully hydrogenated mixture TBA(H)/TOL(H) further support that the elastic intensity of the mixture actually results from the coexistence of two

distinct dynamical contributions, arising respectively from spatially segregated TBA-rich and TOL-rich regions.

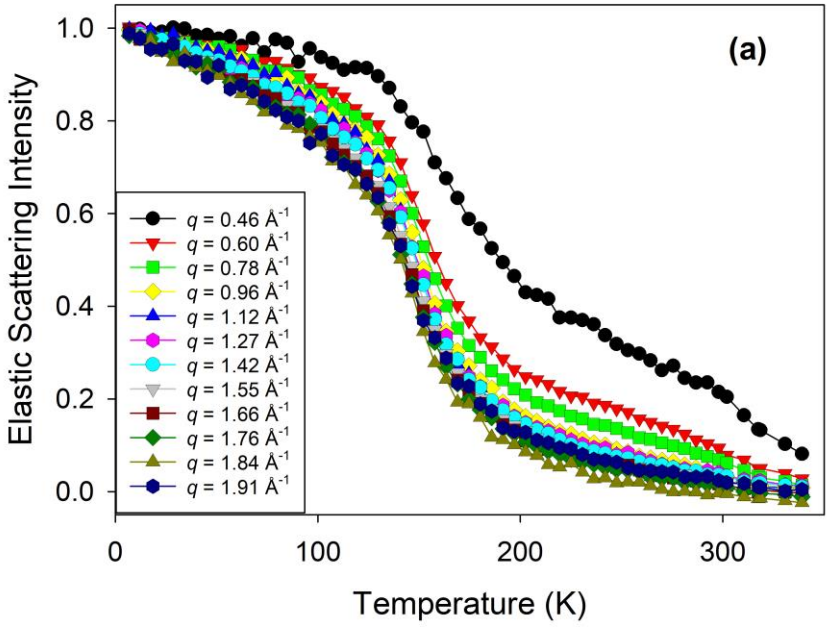

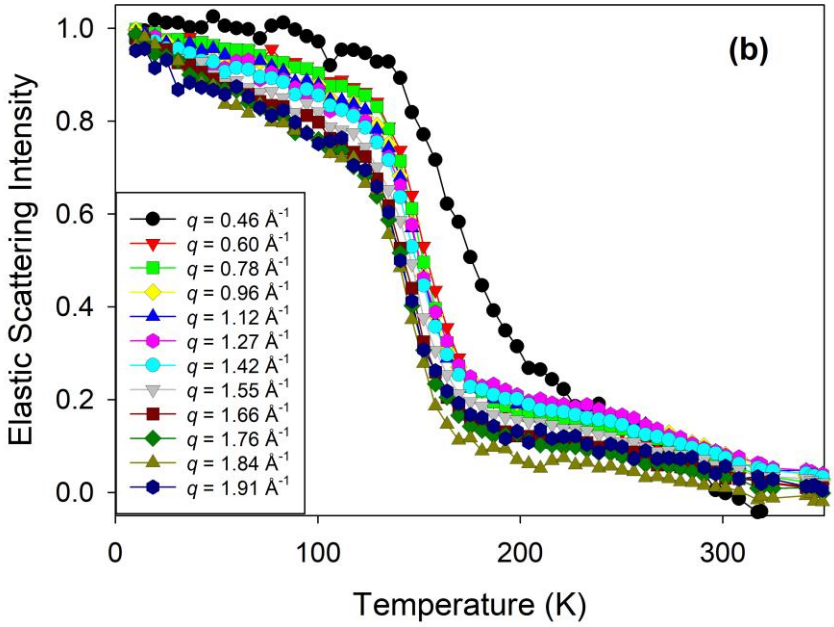
(b)
Elastic Scattering Intensity
Temperature (K)
1.0
0.8
0.6
0.4
0.2
0.0
0
100
200
300
q = 0.46 Å-1
q = 0.60 Å-1
q = 0.78 Å-1
q = 0.96 Å-1
q = 1.12 Å-1
q = 1.27 Å-1
q = 1.42 Å-1
q = 1.55 Å-1
q = 1.66 Å-1
q = 1.76 Å-1
q = 1.84 Å-1
q = 1.91 Å-1

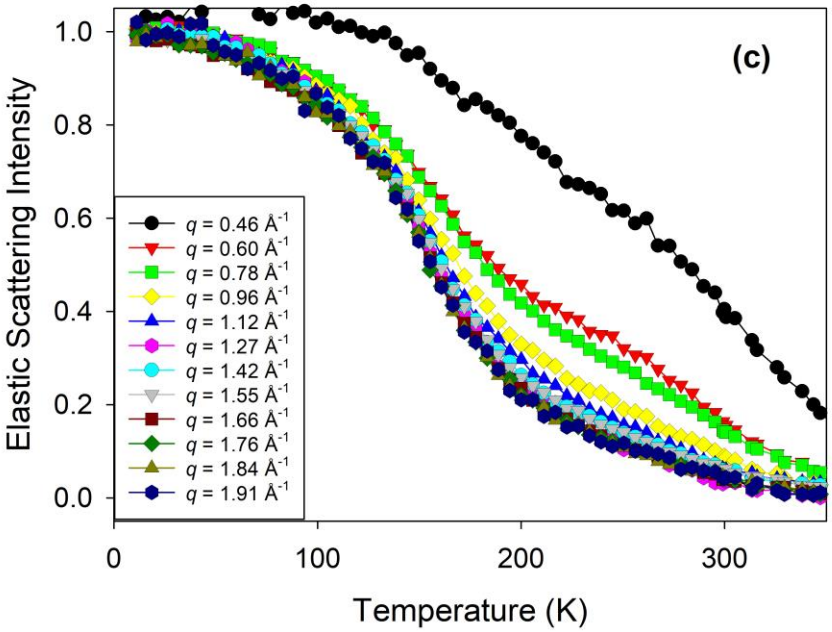
(c)
Elastic Scattering Intensity
Temperature (K)
1.0
0.8
0.6
0.4
0.2
0.0
0
100
200
300
q = 0.46 Å-1
q = 0.60 Å-1
q = 0.78 Å-1
q = 0.96 Å-1
q = 1.12 Å-1
q = 1.27 Å-1
q = 1.42 Å-1
q = 1.55 Å-1
q = 1.66 Å-1
q = 1.76 Å-1
q = 1.84 Å-1
q = 1.91 Å-1

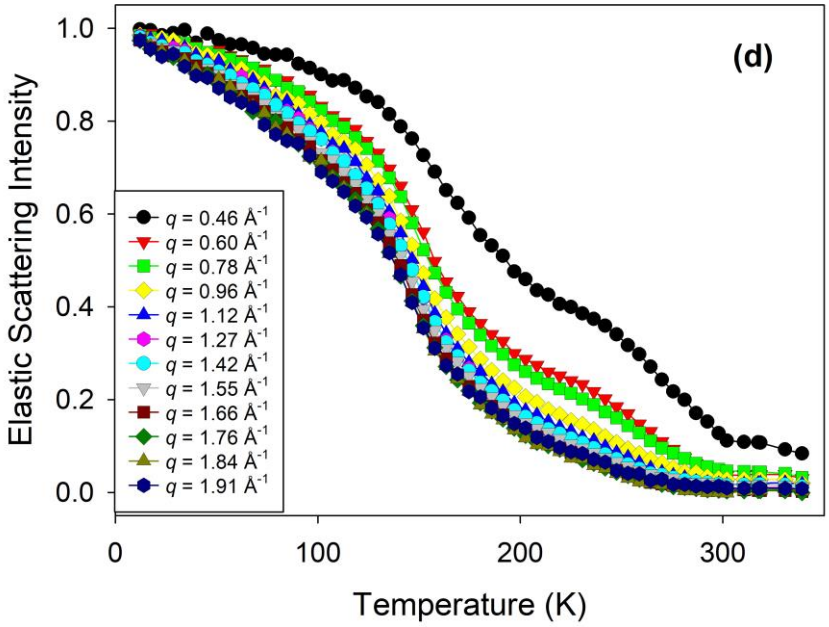

Figure 3. Elastic fixed window scans of the TBA/TOL binary mixtures confined in SBA-15 with a molar fraction of TBA x = 0.5. Keeping the same chemical composition, the mixtures differ in their isotopic composition with (a) TBA(H)/TOL(H), (b) TBA(D)/TOL(H) and (c) TBA(H)/TOL(D). (d) The linear combination of the elastic fixed window scans of the two pure fully hydrogenated liquids for comparison with the actual equimolar mixture (a).

From the Q-dependence of the EFWS one can derive the Mean Square Displacement (MSD), which is a complementary way to study the dynamic structure factor.[40-42] At low temperatures, the quasi-elastic lines related to relaxation processes are sufficiently narrow with respect to the experimental resolution and cannot be distinguished from a true elastic peak. Therefore, setting $S_{quasi}(Q,\omega) = \delta(\omega)$ in Eq.1, it becomes:

$$I^{EFWS}(Q) \propto e^{\frac{-\langle r^2 \rangle Q^2}{6}} \quad (3).$$

The most common procedure used to extract the MSD consists in performing a linear fit of Q^2 versus $\ln(I^{EFWS}(Q))$, where $\langle r^2 \rangle$ is simply deduced from the slope. This analysis is presented in Figures 4a-b for confined TOL and TBA, for a selection of temperatures. It is well-known that this Gaussian law is valid for purely vibrational modes, a situation which is often encountered at low temperature, but deviations are generally observed at increasing temperatures. In our study, one notes that this approximation works well up to about 150 K, as shown in Figures 4a-b. At higher temperature, there is a marked curvature, due to anharmonic effects and the onset of quasi-elastic processes. In addition, the extrapolation of EFWS to $Q = 0$ deviates from unity, a phenomenon that can be enhanced by multiple scattering.

Zorn has shown that EFWSs could still be modelled at a higher temperature if the diffusion processes were taken into account.[43] In this case, the definition of the MSD is extended beyond the simple harmonic case by

$$I^{EFWS}(Q) \propto erfcx(\frac{-\sqrt{\pi}}{2}\frac{\langle r^2 \rangle Q^2}{6}) \quad (4)$$

where *erfcx* is the scaled complementary error function, defined by $erfcx(X) = \exp(X^2)(1 - \mathrm{erf}(X)) = \frac{2}{\sqrt{\pi}}\exp(X^2)\int_X^\infty \exp(-t^2)\,dt$.

Note that in the limit of $\langle r^2 \rangle Q^2 \to 0$, which is applicable at low temperature, this generalized definition of $I^{EFWS}(Q)$ given by Eq. 4 becomes equivalent to the common Gaussian approximation given by Eq. 3.

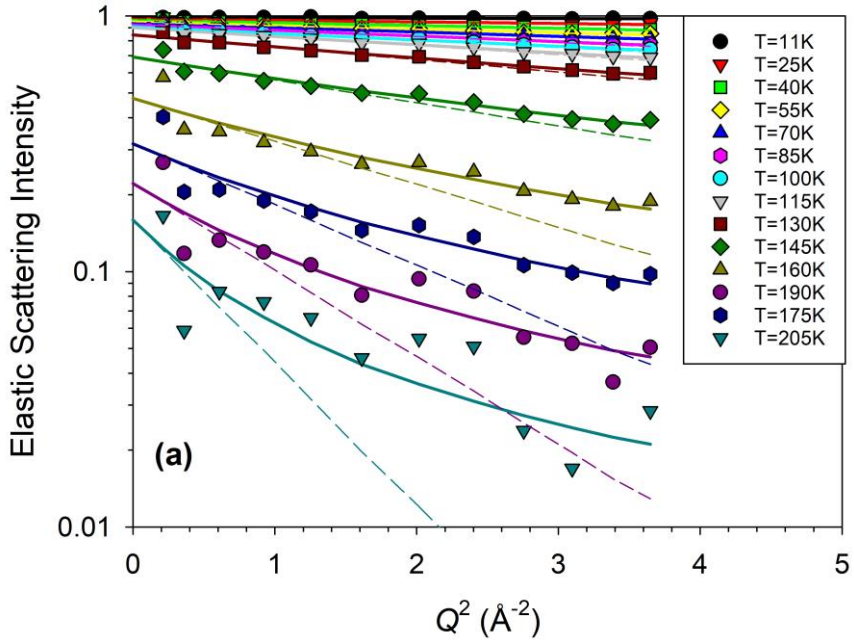
Elastic Scattering Intensity
1
0.1
0.01
0
1
2
3
4
5
Q^2 (Å^{-2})
(a)
T=11K
T=25K
T=40K
T=55K
T=70K
T=85K
T=100K
T=115K
T=130K
T=145K
T=160K
T=190K
T=175K
T=205K

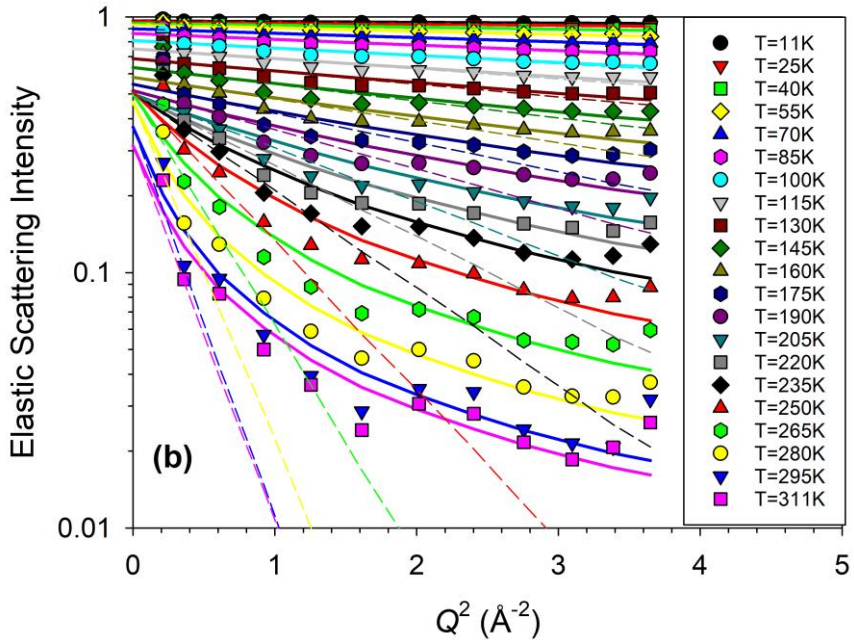
Elastic Scattering Intensity
1
0.1
0.01
0
1
2
3
4
5
Q^2 (Å^{-2})
(b)
T=11K
T=25K
T=40K
T=55K
T=70K
T=85K
T=100K
T=115K
T=130K
T=145K
T=160K
T=175K
T=190K
T=205K
T=220K
T=235K
T=250K
T=265K
T=280K
T=295K
T=311K

Figure 4. Elastic fixed window scans of (a) TOL and (b) TBA confined in SBA-15 at different temperatures. The log-scale of EFWS intensity plotted as a function of the squared momentum transfer emphasizes the temperature range where the usual Gaussian approximation applies (typically for T < 150 K). Fits with the generalized model (solid line) and its low-Q Gaussian approximation (dashed line) are shown. For better clarity, the data shown here are averaged values over 10 successive measurements, so that the temperature step is about 15 K.

Fit curves using this generalized approach are represented by solid lines in Figures 4a-b. Gaussian extrapolations of Eq. 4 to zero *Q* are also indicated by dashed lines. Although the first allowed better adjustments at temperatures above about 150 K, we selected the MSDs derived from the latter procedure to evidence a trend. In what follows, we draw conclusions exclusively from the low temperature range, where the Gaussian approximation is indeed valid and where the intensity of the EFWS is still high (greater than 0.5), assuming that the conditions necessary to ignore secondary contributions to EFWS, such as the coherent scattering and scattering of unlabeled molecules, are met.

Mean Squared Displacement - Experiments. The dynamics of the H-labeled TOL molecules derived from neutron backscattering experiments is illustrated in Figure 5 for different compositions of the binary mixture. Isotopically labeled mixtures of TBA(D)-TOL(H) were used in order to emphasize the mean squared displacement of the H-tagged TOL molecules and to evaluate the effect of the addition of TBA (x_{TBA} = 0, 0.3, 0.5, and 0.7) on the dynamics of TOL.

The MSDs increase almost linearly with the temperature up to about 130 K, where they show a strong increase. The behavior observed in the low temperature region is typical for the vibrational dynamics of solid (glassy) systems and is consistent with the Debye harmonic approximation. The

steep increase above 130 K indicates the onset of local modes with larger amplitudes including librations of molecules and rattling in the neighbor's cage. An influence of the increasing TBA content on the TOLH-MSD could not be determined within the experimental uncertainties, except for the highest TBA fraction at which a small effect is observed above 130 K, as discussed below. Larger mixing effects could have been expected, given that TBA is more viscous than TOL and could have acted as a slowing additive. We infer that this can be rationalized by the concomitance of three facts: first, the core-shell structure adopted by the TBA-TOL mixtures in confinement limits the molecular mixing, so that the TOL environment is maintained in the TOL-rich core region despite dilution. Secondly, the measured MSDs reflect the local dynamics, which is in fact mostly sensitive to the short-ranged environment. Finally, interfacial effects (such as TOL-TBA or TOL-Silica interactions) are presumably low for TOL due to its Van-der-Waals character. Consistently, small BET constants were deduced from the adsorption isotherm experiments of TOL in porous silica.[23]

To conclude the discussion of Figure 5, the observed weaker increase of the TOL MSD near 130 K for x_{TBA} = 0.7 compared to the other three compositions is particularly interesting. Indeed, this suggests that the addition of TBA eventually slows down the dynamics of TOL, at least in the 130-150 K region where the aforementioned precautions concerning the uncertainties of MSDs are properly accounted for. According to the DSC study, this region is located well below the glass transition of TBA. Therefore, we deduce that the reduced large amplitude motions observed for x_{TBA} = 0.7 near 130 K might be a signature of TOL molecules trapped in TBA-rich glassy microdomains. The fact that smaller displacements of TOL are seen only for the largest fraction of TBA, i.e. corresponding to the strongest confinement condition when considering the TBA

surface layer, agrees well with previous observations for pure confined TOL, which indicated that pore diameters as small as 2.4 nm were necessary to significantly affect its glassy dynamics.[7]

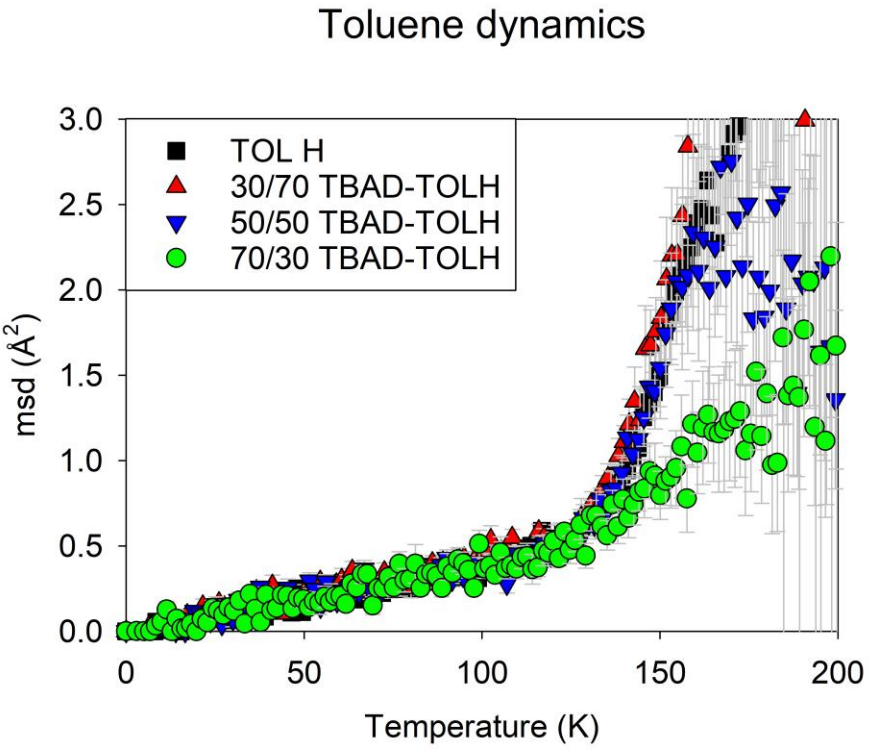

Figure 5. Mean squared displacement of TOL H-tagged-molecules, derived from neutron backscattering experiments on confined TBA(D)-TOL(H) binary mixtures with different compositions (TBA molar fractions x = 0, 0.3, 0.5, and 0.7). The MSD is the result of an analysis with the low Q approximation (see text).

We look now on the opposite labeling, the MSDs of H-tagged TBA molecules confined in SBA-15, which are illustrated in Figure 6. A systematic decrease in MSDs as a function of TOL content is observed in the temperature range of 100 to 150 K. This dependence can be considered as a perfect illustration of the unusual physical behavior of microphase-separated binary fluids because it contradicts interpretations based on simple mixing effects. TOL is a non H-bonding solvent with

a lower viscosity than the H-bonding TBA. According to the usual dilution effects, we could have expected a reduction of the H-bond interactions between the TBA molecules, as shown for bulk mixtures of TBA-TOL,[44] resulting in faster TBA dynamics, as reported for other alcohol-alkane mixtures (Br-butane-butanol mixtures) by NMR and MD simulation.[45] However, this apparently anomalous dilution effect can be easily rationalized by taking the core-shell microstructure of confined TBA-TOL mixtures into account.

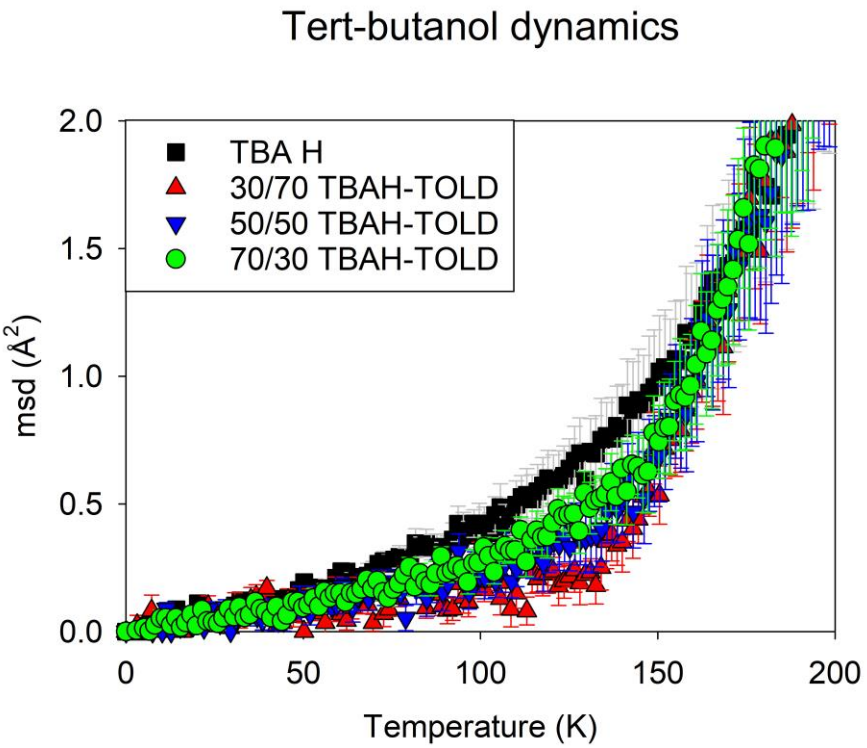

Figure 6. Mean squared displacement of TBA H-tagged-molecules, derived from neutron backscattering experiments for TBA(H)-TOL(D) confined binary mixtures with different compositions (TBA molar fractions x = 1, 0.7, 0.5, and 0.3).

The interpretation is illustrated in Figure 7, where the core-shell structure of TBA-TOL binary mixtures is depicted. It is usually observed that the dynamics of nanoconfined liquids are heterogeneous.[46-49] This fact could be related to the increase in the stretched character of the relaxation function,[50, 51] or equivalently to the temperature broadening (sometimes bimodal) of the glass transition.[7, 39] Dynamic heterogeneities can be related to a wide relaxation times distribution $g(\tau)$, as shown in Figure 7a. While dynamic heterogeneities in supercooled liquids are often described as the coexistence of slow and fast dynamically distinct domains, their spatial nature is more clearly established under confinement. Indeed, surface interactions mostly slow down the mobility of interfacial molecules. The effect of this boundary condition can propagate towards the pore center up to a few molecular sizes.[13, 50, 52, 53]. It can be expected that bulk-like behaviors are recovered sufficiently far from the pore surface. Depending on the ratio between the characteristic length of the interfacial layer and the pore size, a gradient scenario or a two-layers (two-T_gs) scenario can be preferred.[13] The resulting radial distribution of mobility is illustrated in Figure 7b, where the darker the region, the slower its dynamics. The corresponding time τ_{TBA} is plotted in solid white line. In the temperature range 0-200 K, the MSDs measured experimentally are smaller than 3 Å^2, which is negligible compared to the squared pore size (D^2 = 7 000 Å^2). It means that each molecule remains essentially in the same environment on the studied timescale and its MSD reflects the local dynamics. A spatial average results from averaging over molecules which are located at different places in the pore. For pure TBA, the measured EFWS is spatially averaged over the entire pore volume, including both the slower interfacial region and the faster pore center region. In this case a direct experimental disentanglement of both contributions is hardly possible, whereas it is simple by molecular simulation.[52, 54-57]. However, as is illustrated by Figures 7c-d, we demonstrate here that the H-labeling of the TBA molecules makes it possible to highlight the

dynamics of the surface molecules of the core-shell structure which is adopted during the addition of TOL. As a result, the EFWSs measured for TBA(H)/TOL(D) mixtures with an increasing fraction of TOL are particularly sensitive to the slowest part of the relaxation time distribution g(τ), as sketched in Figure 7a. This also rationalizes the apparently counterintuitive "anti-plasticizing effect" of TOL on TBA dynamics.

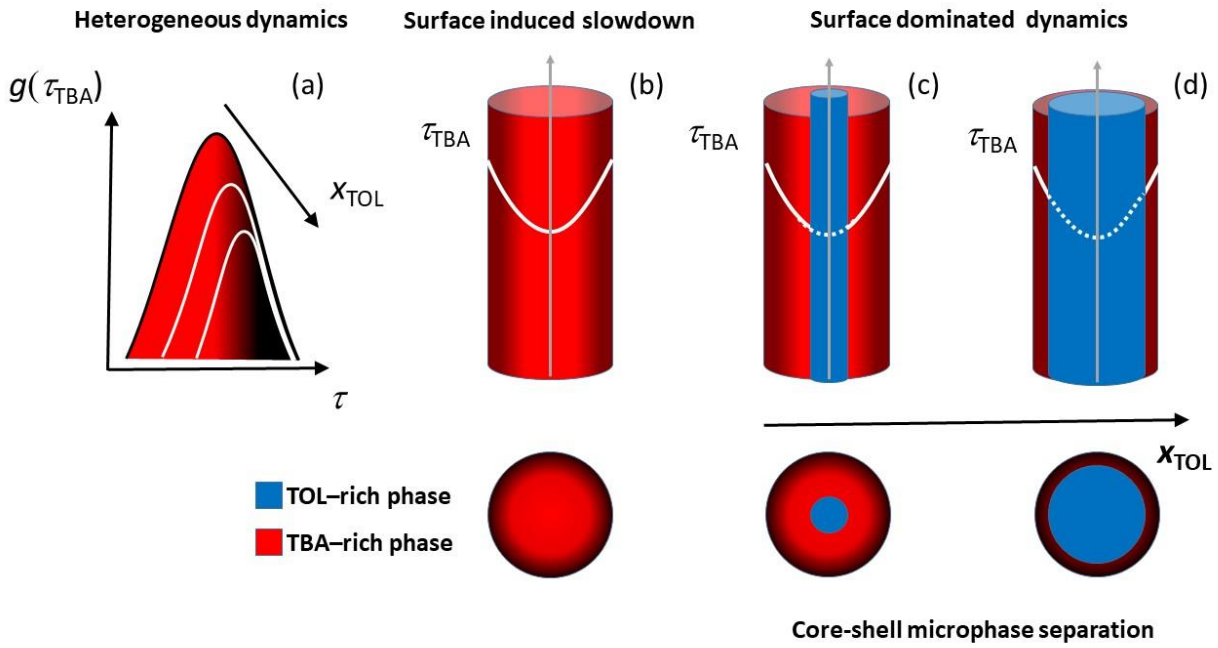

Figure 7. Schematic illustrations of (a) the variation of the relaxation times distribution $g(\tau)$ and (b-d) the dynamical heterogeneities formed by the TBA-rich (in red) and TOL-rich (blue) regions inside a cylindrical nanopore as a function of the volume fraction TOL x_{TOL}. Slower (interfacial) regions are identified by a darker red color.

Mean Squared Displacement – MD Simulation. A molecular simulation study was conducted in order to underline our interpretation of the quasi-elastic neutron scattering experiments. It is based

on a recently published model, capable of reproducing the microphase separation of TBA-TOL mixtures, experimentally demonstrated when confined in silica pore $D = 2.4$ nm.[24] The simulation was performed at a temperature (T = 308 K) significantly higher than that of the experiments in order to guarantee equilibration. Although it prevents us from making a direct quantitative comparison, it allows us to identify the salient features discovered experimentally and to provide them with a microscopic point of view.

The radial density profile of the pure TBA exhibits layering as a function of the distance r from the pore center (cf. Figure 8a), which is a common feature of confined liquids reported by molecular simulation studies.[56, 58] The spatially heterogeneous distribution of molecules was used to distinguish the interfacial layer ($8 < r < 12$ Å) and the central region ($0 < r < 8$ Å). The MSDs of TBA computed for these two regions are illustrated in Figure 8b. The mobility of the interfacial TBA molecules is significantly reduced with respect to the core region, as indicated by an MSD variation of about a factor ten. This observation is consistent with the schematic illustration of Figure 7a. It emphasizes the role of surface interaction, and in particular the formation of H-bonds with surface silanols, on the heterogeneous nature of the dynamics of the confined liquid.

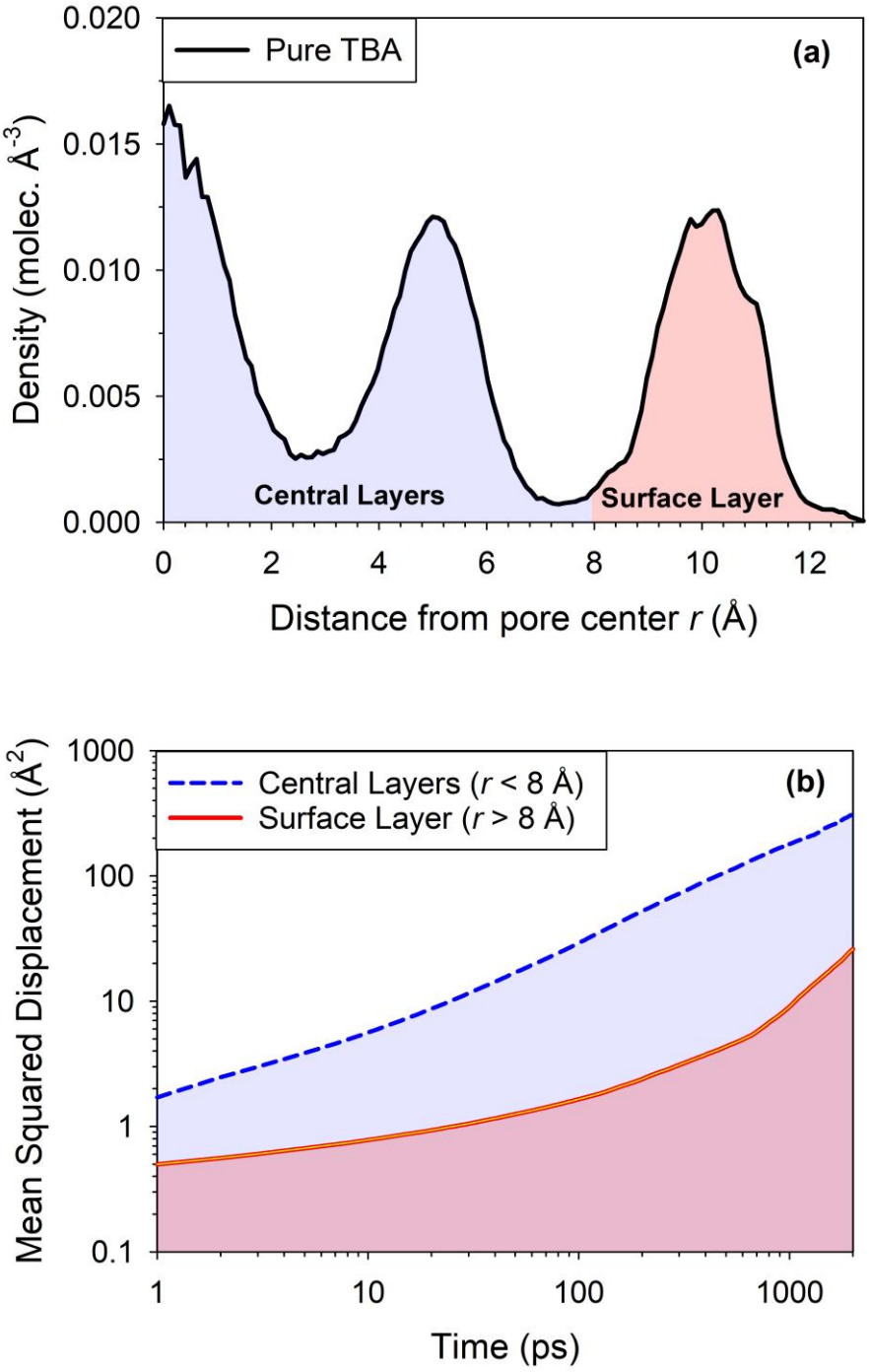

Figure 8. (a) Radial density profile of the center of mass of pure TBA confined in nanoporous silica at 308 K, and (b) MSD of TBA molecules as a function of their distance from the pore center, dashed line : pore center region ($0 < r < 8$ Å), solid line : surface layer : ($8 < r < 12$ Å).

The structure adopted by the binary mixture (x_{TBA} = 0.24) is illustrated in Figure 9a by the radial density profiles of the two molecules. Segregation of the two components is observed, leading to a core-shell structure where the TBA molecules are preferentially located at the pore surface and TOL at the center of the pore. This microphase separation is driven by the different strength of the liquid-surface interactions of TBA and TOL molecules, as indicated in previous studies.

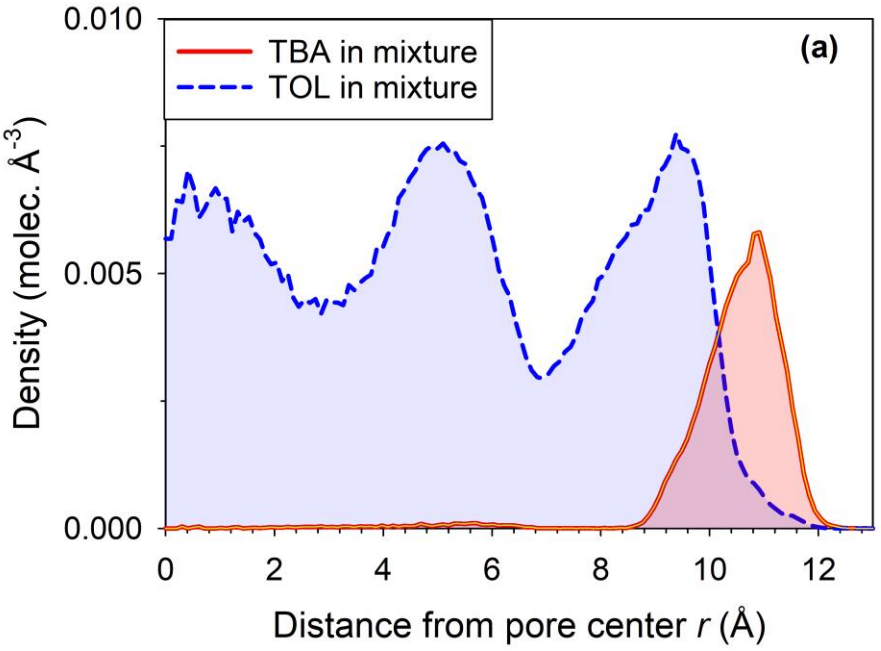

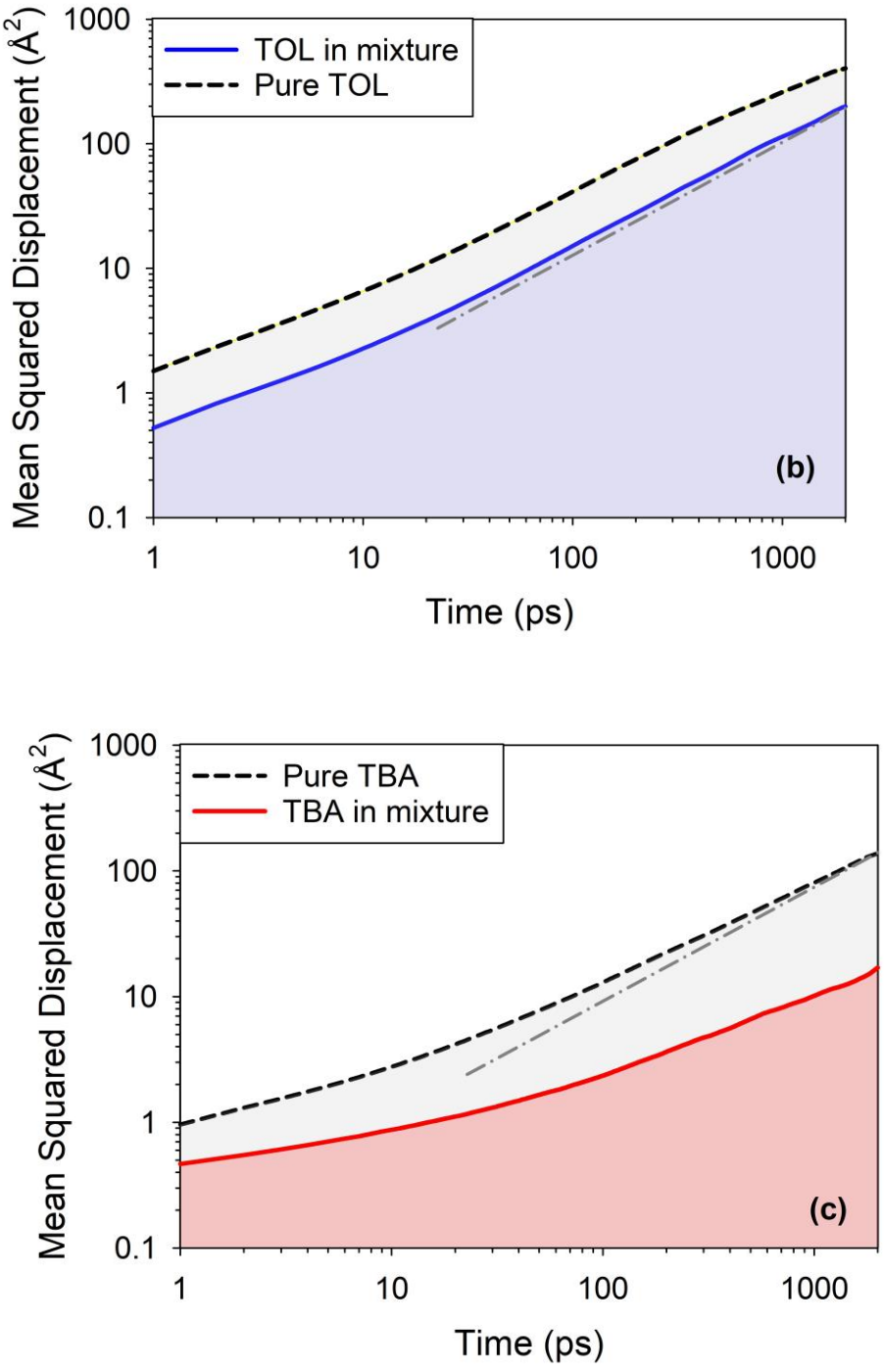

Figure 9. (a) Radial density profile of the center of mass of TBA (solid line) and TOL (dashed line) molecules in the confined binary mixture (x_{TBA} = 0.24). (b) MSD of TOL molecules in the

pure (dashed line) and in the binary mixture (solid line), and (c) MSD of TBA molecules in the pure (dashed line) and in the binary mixture (solid line). The dashed-dotted line is a guideline with a linear slope corresponding to the diffusive behavior.

The time dependent MSDs of the TOL and TBA molecules are illustrated in Figures 9b and c, respectively. These are simulated counterparts of experimental the EFWS (corresponding to several nanoseconds) with H-labeled molecules. The dynamics of TOL in pure and binary liquids are qualitatively similar. Specifically, the MSDs of both samples present a linear dependence on time (indicated by a dashed-dotted line), which indicates the normal Fick diffusion law. Slightly slower dynamics are witnessed for the mixture, which is demonstrated by a reduction in the MSD by a factor of two. This suggests that, due to the microsegregation phenomenon, the local environment of the TOL molecules is maintained in the binary liquid, and thus its dynamics are weakly affected. This is in agreement with the experiments discussed above. A slight deceleration may indicate a weak coupling of the TOL mobility with the slower dynamics of TBA, but this could also originate from the stronger effective confinement imposed by the non-moving shell on the liquid core. It is interesting to note that the dynamics of the TBA varies considerably with the addition of TOL, as shown in Figure 9c, where the MSD is reduced by one order of magnitude. Moreover, the TBA dynamics exhibit a clear sub-diffusive character in the confined mixture, while obeying a Fick law in the pure liquid form. It should be emphasized again that this behavior is in contradiction with the simple mixing effect (plasticizing) of TOL on TBA. In fact, the MSDs of TBA in the mixture demonstrate values similar to those of the contact layer in the pure component. This supports our understanding that the unexpected dynamics of TBA is closely related to the core-shell structure adopted by binary liquids under confinement.

CONCLUSIONS

The dynamics of binary liquids confined in the straight and monodispersed channels of ordered SBA-15 mesoporous materials were investigated by elastic fixed window scans to probe nanosecond timescales. Pure components as well as different binary mixtures were studied in which selective isotopic labeling was used to highlight the dynamics of the hydrogenated component. Mean squared displacements were acquired from the *Q*-dependence of the EFWS scans, and their interpretation was substantiated by the results of MD simulation.

According to the experiments carried out on the various TBA(D)/TOL(H) mixtures, it appears that the dynamics of TOL does not vary significantly with the addition of TBA. This behavior corroborates the poor mixing of both components in confined geometry, as also indicated by the observation of two distinct glass transitions and previously published structural studies. Furthermore, the experiments on the various TBA(H)/TOL(D) mixtures indicate a reduction of the MSDs of TBA when the fraction of TOL increases. Since TOL is a non-H-bonded additive with a glass transition temperature much lower than that of TBA, this observed impact on TBA dynamics cannot be understood by simple mixing rules. On the contrary, we propose a simple rationalization of this counterintuitive behavior based on the microscopic pictures provided by MD simulation, and by taking into account the specific nature of nanoconfined binary liquids and their recently discovered tendency to form core-shell microphase separated structures.[22] For the pure liquid, the measured mobility of TBA reflects a spatial average on dynamic heterogeneities ranging from the center of the pore to the pore wall, whereas for the binary systems, the core-shell structure makes it specifically representative of the interfacial molecules of TBA. Due to the strong interaction between silica and TBA molecules induced by the formation of H-bonds, it is logical that the

dynamics of interfacial molecules probed for TBAH/TOLD mixtures represent the slowest tail of the relaxation times distribution of the confined liquid.

These findings verify and confirm from a dynamic point of view the structure proposed by the modeling of small angle neutron scattering data.[22] To our knowledge, this combination of direct experimental studies on confinement-induced microphase separated liquids both from a structural and a dynamic point of view is rather unique in literature. We therefore expect that this approach will help to better understand other cases discussed in the literature in which dynamic evidences of microphase demixing are reported.[16-18, 59, 60]

It is worth noting that this study gives a clearer insight on the nature of the dynamic heterogeneities, which have also been observed for the same liquids confined in the smaller pores of MCM-41 materials by calorimetry.[25] Beyond those calorimetric results, the interpretation of which being limited by the absence of chemical selectivity of DSC, the significance of this study lies in its ability to make a real distinction between the dynamics of the two molecular components (TBA and TOL molecules) constituting the confined binary mixtures. In addition to MD simulation, one cannot ignore the exceptional value of neutron scattering methods with component-selective H/D labeling in providing a direct correlation between spatially segregated dynamical heterogeneities and the formation of original core-shell nanostructures. These critical findings call for further investigations. Beyond the need to extent the study to different systems and timescale, a subsequent quantitative dynamic analysis remains essential for a full insight on the physical behavior of such complex systems under confinement.

ACKNOWLEDGMENTS

The experiments were performed in the frame of the PhD project of R. Mhanna who acknowledges funding by the Institute Laue-Langevin and the Brittany Region (ARED 7784 / NanoBina). Support from Europe (FEDER) and Rennes Metropole is expressly acknowledged. This project has received funding from the European Union's 7th Framework Programme for research, technological development and demonstration under the NMI3-II Grant number 283883. We thank Odile MERDRIGNAC (Institut des Sciences Chimiques de Rennes) for her assistance with Nitrogen isotherms experiments for the characterization of the SBA-15 materials.

REFERENCES:

1. Jackson, C.; McKenna, G., The Glass-Transition of Organic Liquids Confined to Small Pores. *Journal of Non-Crystalline Solids* **1991,** *131,* 221-224.

2. Granick, S., Motions and Relaxations of Confined Liquids. *Science* **1991,** *253* (5026), 1374-1379.

3. Zhang, J.; Liu, G.; Jonas, J., Effects of Confinement on the Glass-Transition Temperature of Molecular Liquids. *Journal of Physical Chemistry* **1992,** *96* (8), 3478-3480.

4. Arndt, M.; Stannarius, R.; Gorbatschow, W.; Kremer, F., Dielectric Investigations of the Dynamic Glass Transition in Nanopores. *Physical Review E* **1996,** *54* (5), 5377-5390.

5. Schuller, J.; Melnichenko, Y.; Richert, R.; Fischer, E., Dielectric Studies of the Glass Transition in Porous Media. *Physical Review Letters* **1994,** *73* (16), 2224-2227.

6. Christenson, H. K., Confinement Effects on Freezing and Melting. *Journal of Physics-Condensed Matter* **2001,** *13* (11), R95-R133.

7. Morineau, D.; Xia, Y. D.; Alba-Simionesco, C., Finite-Size and Surface Effects on the Glass Transition of Liquid Toluene Confined in Cylindrical Mesopores. *Journal of Chemical Physics* **2002,** *117* (19), 8966-8972.

8. Alba-Simionesco, C.; Dosseh, G.; Dumont, E.; Frick, B.; Geil, B.; Morineau, D.; Teboul, V.; Xia, Y., Confinement of Molecular Liquids: Consequences on Thermodynamic, Static and Dynamical Properties of Benzene and Toluene. *European Physical Journal E* **2003,** *12* (1), 19-28.

9. Morineau, D.; Alba-Simionesco, C., Liquids in Confined Geometry: How to Connect Changes in the Structure Factor to Modifications of Local Order. *Journal of Chemical Physics* **2003,** *118* (20), 9389-9400.

10. Alcoutlabi, M.; McKenna, G. B., Effects of Confinement on Material Behaviour at the Nanometre Size Scale. *Journal of Physics-Condensed Matter* **2005,** *17* (15), R461-R524.

11. Alba-Simionesco, C.; Coasne, B.; Dosseh, G.; Dudziak, G.; Gubbins, K. E.; Radhakrishnan, R.; Sliwinska-Bartkowiak, M., Effects of Confinement on Freezing and Melting. *Journal of Physics-Condensed Matter* **2006,** *18* (6), R15-R68.

12. Morineau, D.; Alba-Simionesco, C., Does Molecular Self-Association Survive in Nanochannels? *Journal of Physical Chemistry Letters* **2010,** *1* (7), 1155-1159.

13. Richert, R., Dynamics of Nanoconfined Supercooled Liquids. *Annual Review of Physical Chemistry, Vol 62* **2011,** *62*, 65-84.

14. Huber, P., Soft Matter in Hard Confinement: Phase Transition Thermodynamics, Structure, Texture, Diffusion and Flow in Nanoporous Media. *Journal of Physics-Condensed Matter* **2015,** *27* (10).

15. Audonnet, F.; Brodie-Linder, N.; Morineau, D.; Frick, B.; Alba-Simionesco, C., From the Capillary Condensation to the Glass Transition of a Confined Molecular Liquid: Case of Toluene. *Journal of Non-Crystalline Solids* **2015,** *407*, 262-269.

16. Elamin, K.; Jansson, H.; Kittaka, S.; Swenson, J., Different Behavior of Water in Confined Solutions of High and Low Solute Concentrations. *Physical Chemistry Chemical Physics* **2013,** *15* (42), 18437-18444.

17. Swenson, J.; Elamin, K.; Chen, G.; Lohstroh, W.; Sakai, V. G., Anomalous Dynamics of Aqueous Solutions of di-Propylene Glycol Methylether Confined in MCM-41 by Quasielastic Neutron Scattering. *Journal of Chemical Physics* **2014,** *141* (21).

18. Elamin, K.; Jansson, H.; Swenson, J., Dynamics of Aqueous Binary Glass-Formers Confined in MCM-41. *Physical Chemistry Chemical Physics* **2015,** *17* (19), 12978-12987.

19. Hamid, A.; Lefort, R.; Lechaux, Y.; Moreac, A.; Ghoufi, A.; Alba-Simionesco, C.; Morineau, D., Solvation Effects on Self-Association and Segregation Processes in tert-Butanol-Aprotic Solvent Binary Mixtures. *Journal of Physical Chemistry B* **2013,** *117* (35), 10221-10230.

20. Mhanna, R.; Lefort, R.; Noirez, L.; Morineau, D., Microstructure and Concentration Fluctuations in Alcohol-Toluene and Alcohol-Cyclohexane Binary Liquids: A Small Angle Neutron Scattering Study. *Journal of Molecular Liquids* **2016,** *218*, 198-207.

21. Hamid, A. R. A.; Mhanna, R.; Lefort, R.; Ghoufi, A.; Alba-Simionesco, C.; Frick, B.; Morineau, D., Microphase Separation of Binary Liquids Confined in Cylindrical Pores. *Journal of Physical Chemistry C* **2016,** *120* (17), 9245-9252.

22. Mhanna, R.; Hamid, A.; Dutta, S.; Lefort, R.; Noirez, L.; Frick, B.; Morineau, D., More Room for Microphase Separation: An Extended Study on Binary Liquids Confined in SBA-15 Cylindrical Pores. *Journal of Chemical Physics* **2017,** *146* (2).

23. Dutta, S.; Lefort, R.; Morineau, D.; Mhanna, R.; Merdrignac-Conanec, O.; Saint-Jalmes, A.; Leclercq, T., Thermodynamics of Binary Gas Adsorption in Nanopores. *Physical Chemistry Chemical Physics* **2016,** *18* (35), 24361-24369.

24. Essafri, I.; Morineau, D.; Ghoufi, A., Microphase Separation of a Miscible Binary Liquid Mixture under Confinement at the Nanoscale. *Npj Computational Materials* **2019,** *5*.

25. Hamid, A. R. A.; Mhanna, R.; Catrou, P.; Bulteau, Y.; Lefort, R.; Morineau, D., Multiple Glass Transitions of Microphase Separated Binary Liquids Confined in MCM-41. *Journal of Physical Chemistry C* **2016,** *120* (20), 11049-11053.

26. Zhao, D.; Huo, Q.; Feng, J.; Chmelka, B.; Stucky, G., Nonionic Triblock and Star Diblock Copolymer and Oligomeric Surfactant Syntheses of Highly Ordered, Hydrothermally Stable, Mesoporous Silica Structures. *Journal of the American Chemical Society* **1998,** *120* (24), 6024-6036.

27. Dosseh, G.; Brodie-Linder, N.; Frick, B.; Le Quellec, C.; Morineau, D.; Alba-Simionesco, C., Dynamical Properties of Toluene and ortho-Terphenyl Confined in MCM-41 and SBA-15 Mesoporous Materials. *Annales De Chimie-Science Des Materiaux* **2005,** *30* (4), 365-373.

28. Xia, Y. D.; Dosseh, G.; Morineau, D.; Alba-Simionesco, C., Phase Diagram and Glass Transition of Confined Benzene. *Journal of Physical Chemistry B* **2006,** *110* (39), 19735-19744.

29. Brodie-Linder, N.; Dosseh, G.; Alba-Simonesco, C.; Audonnet, F.; Imperor-Clerc, M., SBA-15 synthesis: Are there Lasting Effects of Temperature Change within the First 10 min of TEOS Polymerization? *Materials Chemistry and Physics* **2008,** *108* (1), 73-81.

30. Wuttke, J.; Budwig, A.; Drochner, M.; Kammerling, H.; Kayser, F.; Kleines, H.; Ossovyi, V.; Pardo, L.; Prager, M.; Richter, D.; Schneider, G.; Schneider, H.; Staringer, S., SPHERES, Julich's High-Flux Neutron Backscattering Spectrometer at FRM II. *Review of Scientific Instruments* **2012,** *83* (7).

31. Michaela, Z.; Marina, K., SPHERES: Backscattering Spectrometer. *Journal of large-scale research facilities* **2015,** *A30*, 1-4.

32. Brodka, A.; Zerda, T., Properties of Liquid Acetone in Silica Pores: Molecular Dynamics Simulation. *Journal of Chemical Physics* **1996,** *104* (16), 6319-6326.

33. Cygan, R.; Liang, J.; Kalinichev, A., Molecular Models of Hydroxide, Oxyhydroxide, and Clay Phases and the Development of a General Force Field. *Journal of Physical Chemistry B* **2004,** *108* (4), 1255-1266.

34. Jorgensen, W.; Maxwell, D.; TiradoRives, J., Development and Testing of the OPLS All-Atom Force Field on Conformational Energetics and Properties of Organic Liquids. *Journal of the American Chemical Society* **1996,** *118* (45), 11225-11236.

35. Forester, T. R.; Smith, W. DLPOLY, CCP5 Program Library; Daresbury Lab., Warrington, 2004.

36. Melchionna, S.; Ciccotti, G.; Holian, B., Hoover NPT Dynamics for Systems Vayring in Shape and Size. *Molecular Physics* **1993,** *78* (3), 533-544.

37. Smith, W.; Forester, T., DL_POLY_2.0: A General-Purpose Parallel Molecular Dynamics Simulation Package. *Journal of Molecular Graphics* **1996,** *14* (3), 136-141.

38. McGregor, P. A.; Allan, D. R.; Parsons, S.; Clark, S. J., Hexamer Formation in Tertiary Butyl Alcohol (2-Methyl-2-Propanol, C4H10O). *Acta Crystallographica Section B-Structural Science* **2006,** *62*, 599-605.

39. Le Quellec, C.; Dosseh, G.; Audonnet, F.; Brodie-Linder, N.; Alba-Simionesco, C.; Haussler, W.; Frick, B., Influence of Surface Interactions on the Dynamics of the Glass Former ortho-Terphenyl Confined in Nanoporous Silica. *European Physical Journal-Special Topics* **2007,** *141*, 11-18.

40. Marc, B., *Quasi-elastic Neutron Scattering Principles and Application in Solid State Chemistry, Biology and Materials Science*. Adam Hilger, Bristol ed.; 1998.

41. Guégan, R.; Morineau, D.; Lefort, R.; Moréac, A.; Béziel, W.; Guendouz, M.; Zanotti, J. M.; Frick, B., Molecular Dynamics of a Short-Range Ordered Smectic Phase Nanoconfined in Porous Silicon. *Journal of Chemical Physics* **2007,** *126* (6).

42. Ndao, M.; Lefort, R.; Cerclier, C.; Busselez, R.; Morineau, D.; Frick, B.; Ollivier, J.; Kityk, A.; Huber, P., Molecular Dynamics of Pyrene Based Discotic Liquid Crystals Confined in Nanopores Probed by Incoherent Quasielastic Neutron Scattering. *Rsc Advances* **2014,** *4* (103), 59358-59369.

43. Zorn, R., On the Evaluation of Neutron Scattering Elastic Scan Data. *Nuclear Instruments & Methods in Physics Research Section a-Accelerators Spectrometers Detectors and Associated Equipment* **2009,** *603* (3), 439-445.

44. Hamid, A. R. A.; Lefort, R.; Lechaux, Y.; Moreac, A.; Ghoufi, A.; Alba-Simionesco, C.; Morineau, D., Solvation Effects on Self-Association and Segregation Processes in tert-Butanol-Aprotic Solvent Binary Mixtures. *Journal of Physical Chemistry B* **2013,** *117* (35), 10221-10230.

45. Hennous, L.; Hamid, A.; Lefort, R.; Morineau, D.; Malfreyt, P.; Ghoufi, A., Crossover in Structure and Dynamics of a Primary Alcohol Induced by Hydrogen-Bonds Dilution. *Journal of Chemical Physics* **2014,** *141* (20).

46. Donth, E., The Size of Cooperatively Rearranging Regions at the Glass-Transition. *Journal of Non-Crystalline Solids* **1982,** *53* (3), 325-330.

47. Ediger, M. D.; Angell, C. A.; Nagel, S. R., Supercooled Liquids and Glasses. *Journal of Physical Chemistry* **1996,** *100* (31), 13200-13212.

48. Tracht, U.; Wilhelm, M.; Heuer, A.; Feng, H.; Schmidt-Rohr, K.; Spiess, H. W., Length Scale of Dynamic Heterogeneities at the Glass Transition Determined by

Multidimensional Nuclear Magnetic Resonance. *Physical Review Letters* **1998,** *81* (13), 2727-2730.

49. Ediger, M., Spatially Heterogeneous Dynamics in Supercooled Liquids. *Annual Review of Physical Chemistry* **2000,** *51*, 99-128.

50. Zorn, R.; Hartmann, L.; Frick, B.; Richter, D.; Kremer, F., Inelastic Neutron Scattering Experiments on the Dynamics of a Glass-Forming Material in Mesoscopic Confinement. *Journal of Non-Crystalline Solids* **2002,** *307*, 547-554.

51. Dosseh, G.; Le Quellec, C.; Brodie-linder, N.; Alba-simionesco, C.; Haeussler, W.; Levitz, P., Fluid-Wall Interactions Effects on the Dynamical Properties of Confined Orthoterphenyl. *Journal of Non-Crystalline Solids* **2006,** *352* (42-49), 4964-4968.

52. Scheidler, P.; Kob, W.; Binder, K., Cooperative Motion and Growing Length Scales in Supercooled Confined Liquids. *Europhysics Letters* **2002,** *59* (5), 701-707.

53. Lefort, R.; Morineau, D.; Guegan, R.; Guendouz, M.; Zanotti, J. M.; Frick, B., Relation between Static Short-range Order and Dynamic Heterogeneities in a Nanoconfined Liquid Crystal. *Physical Review E* **2008,** *78* (4).

54. Scheidler, P.; Kob, W.; Binder, K., The Relaxation Dynamics of a Confined Glassy Simple Liquid. *European Physical Journal E* **2003,** *12* (1), 5-9.

55. Ji, Q.; Lefort, R.; Busselez, R.; Morineau, D., Structure and Dynamics of a Gay-Berne Liquid Crystal Confined in Cylindrical Nanopores. *Journal of Chemical Physics* **2009,** *130* (23).

56. Busselez, R.; Lefort, R.; Ji, Q.; Affouard, F.; Morineau, D., Molecular Dynamics Simulation of Nanoconfined Glycerol. *Physical Chemistry Chemical Physics* **2009,** *11* (47), 11127-11133.

57. Ghoufi, A.; Hureau, I.; Morineau, D.; Renou, R.; Szymczyk, A., Confinement of tert-Butanol Nanoclusters in Hydrophilic and Hydrophobic Silica Nanopores. *Journal of Physical Chemistry C* **2013,** *117* (29), 15203-15212.

58. Guégan, R.; Morineau, D.; Alba-Simionesco, C., Interfacial Structure of an H-Bonding Liquid Confined into Silica Nanopore with Surface Silanols. *Chemical Physics* **2005,** *317* (2-3), 236-244.

59. Guo, X. Y.; Watermann, T.; Sebastiani, D., Local Microphase Separation of a Binary Liquid under Nanoscale Confinement. *Journal of Physical Chemistry B* **2014,** *118* (34), 10207-10213.

60. Lerbret, A.; Lelong, G.; Mason, P. E.; Saboungi, M. L.; Brady, J. W., Molecular Dynamics and Neutron Scattering Study of Glucose Solutions Confined in MCM-41. *Journal of Physical Chemistry B* **2011,** *115* (5), 910-918.

TOC GRAPHIC

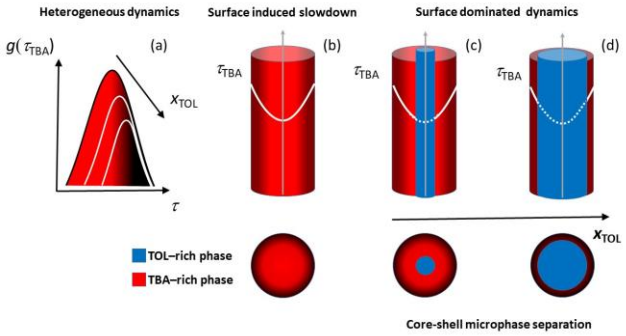
Heterogeneous dynamics
Surface induced slowdown
Surface dominated dynamics
g(τTBA)
(a)
(b)
(c)
(d)
τTBA
xTOL
τ
TOL–rich phase
TBA–rich phase
Core-shell microphase separation